A numerical study of the Southwestern Atlantic Shelf circulation: Barotropic response to tidal and wind forcing

Elbio D. Palma[1]
Departamento de Física, Universidad Nacional del Sur, Bahía Blanca, Argentina

Ricardo P. Matano
College of Oceanic and Atmospheric Sciences, Oregon State University, Corvallis, Oregon, USA

Alberto R. Piola[2]
Departamento de Oceanografía, Servicio de Hidrografía Naval, Buenos Aires, Argentina

Received 8 February 2004; revised 16 April 2004; accepted 13 May 2004; published 20 August 2004.

[1] This article analyzes the barotropic circulation in the Southwestern Atlantic Shelf using a three-dimensional numerical model forced with winds and tides. South of 40°S, the shelf circulation is dominated by the propagation of the semidiurnal tides. In this region the diurnal tides are generally weak, except at the shelf edge where they resonate with northward propagating, continental shelf waves. North of 40°S, the tidal circulation is relatively weak, and the circulation is mainly driven by the winds. The wind-driven annual mean circulation is characterized by a broad northeastward flow south of approximately 40°S and is characterized by a southwestward flow farther north. The intense mixing associated with the Patagonian tides enhances the bottom friction that balances the energy input from the wind stress forcing. In contrast with previous results our simulation shows a detrainment of the northward volume transport with latitude due to an offshore flow along the edge of the Patagonian shelf break. The largest seasonal variations of the shelf circulation are observed in the region between 45°S and 25°S where, during the fall, there is a development of a clockwise gyre and a northeastward flow north of 40°S. The gyre weakens toward the winter, and the northeastward flow reverses directions. *INDEX TERMS:* 4255 Oceanography: General: Numerical modeling; 4219 Oceanography: General: Continental shelf processes; 4560 Oceanography: Physical: Surface waves and tides (1255); *KEYWORDS:* shelf circulation, numerical modeling, tidal and wind forcing

Citation: Palma, E. D., R. P. Matano, and A. R. Piola (2004), A numerical study of the Southwestern Atlantic Shelf circulation: Barotropic response to tidal and wind forcing, *J. Geophys. Res.*, *109*, C08014, doi:10.1029/2004JC002315.

1. Introduction

[2] The Southwestern Atlantic Shelf (SWAS) is the largest continental shelf of the Southern Hemisphere [*Bisbal*, 1995]. It extends from the Burdwood Bank, Argentina (55°S), to Cabo Frío, Brazil (23°S) (Figure 1). The shelf region is relatively narrow in the north (~70 km in southern Brazil and Uruguay) and widens to the south (~850 km in southern Argentina). The circulation of this vast region depends on the propagation of tidal waves, wind forcing, freshwater discharges, and the influence of neighboring western boundary currents (Figure 1). The relative contribution of each of these forcings to the circulation patterns varies among regions. South of 40°S, a region known as the Patagonian Shelf, the circulation is dominated by tidal forcing and strong offshore winds, while farther north, in the Brazilian sector, it is dominated by the poleward flow of the Brazil Current and the freshwater discharges from the Río de la Plata and the Lagoa dos Patos. Although wind forcing is thought to be important everywhere, its contribution to the overall circulation is far from clear. In fact, the local wind response is overshadowed by anomalously large tidal currents south of 40°S and by the proximity of the neighboring western boundary flows farther north.

[3] Owing to the scarcity of observations most descriptions of the SWAS circulation have been focused on relatively small areas [e.g., *Rivas and Frank Langer*, 1996; *Martos and Piccolo*, 1988; *Lima et al.*, 1996; *Piola et al.*, 2000; *Zavialov et al.*, 2002]. The lack of observations has also hampered the development and testing of numerical studies, which remain few, circumscribed to small subregions of the SWAS and generally focused in one portion of the forcing mechanisms (e.g., wind or tides) [*Glorioso and Flather*, 1995, 1997; *Forbes and Garraffo*, 1988; *Pereira*,

[1] Also at Instituto Argentino de Oceanografía, Bahía Blanca, Argentina.
[2] Also at Departamento de Ciencias de la Atmósfera y los Océanos, Universidad de Buenos Aires, Buenos Aires, Argentina, and Instituto Argentino de Oceanografía, Bahía Blanca, Argentina.

0148-0227/04/2004JC002315$09.00

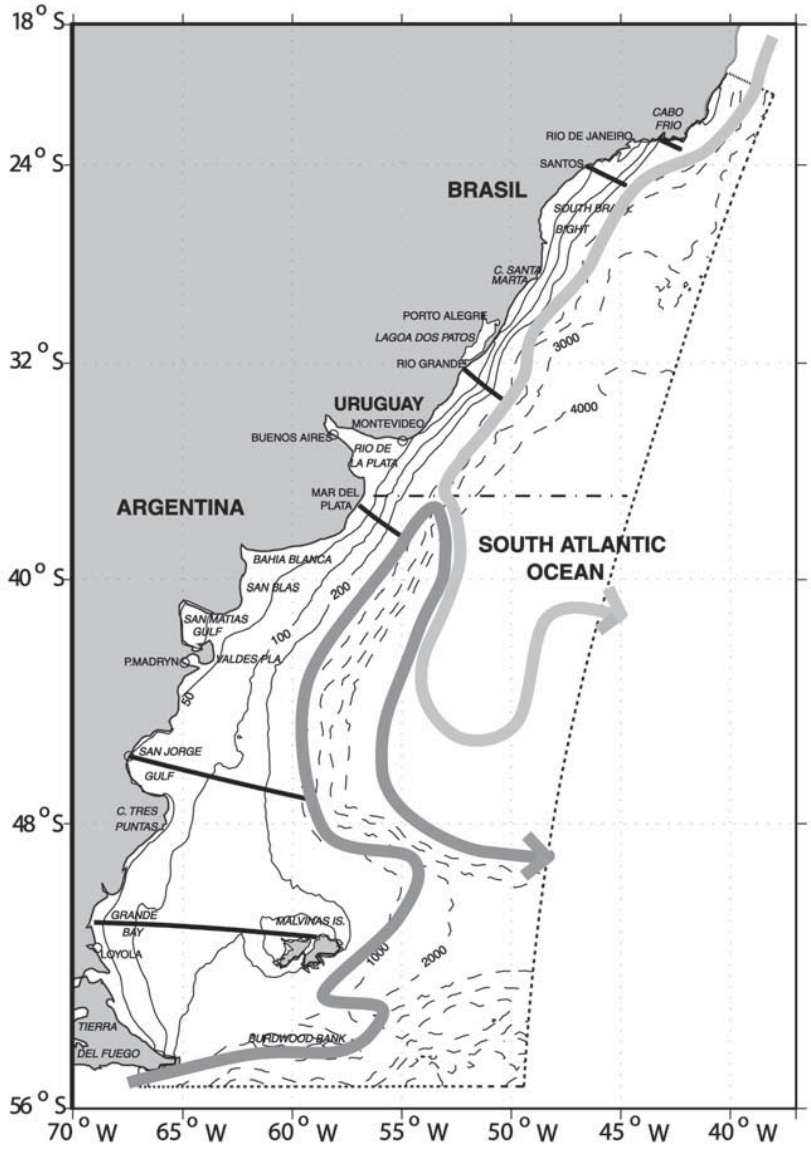

Figure 1. Map showing the bathymetry and geographical locations referred to in the text. Solid lines show 50-, 100-, and 200-m contours; dashed lines show 1000-, 2000-, 3000-, and 4000-m contours. The dotted line indicates the offshore limits of the model. The dark shaded line is the schematic path of the Malvinas Current; the light shaded line is the path of the Brazil Current. Heavy solid lines indicate cross sections, and the horizontal dotted-dashed line at 37°S indicates the artificial limit between the Patagonian Shelf and the northern shelf employed in the discussion of model results.

1989; *Rodrigues and Lorenzetti*, 2001]. Although these studies have greatly improved our understanding of the regional circulation, they have not been able to address the more realistic scenario of a three-dimensional (3-D), baroclinic shelf circulation forced by winds, tides, and freshwater discharges and subject to the influence of neighboring western boundary flows.

[4] The rapid increase of computing capability of recent years allows us to build upon previous work and extend those studies to include hitherto unexplored effects in a suite of numerical experiments encompassing the SWAS region. To facilitate the dynamical understanding of these results, our experimental strategy was to start with the simplest of the cases, a three-dimensional barotropic version of the SWAS forced by wind and tides, and to progress to the more complex case of a realistically density-stratified shelf forced also by freshwater discharges and western boundary currents. The magnitude of the information contained in these experiments is too large to be conveyed in a single article; therefore the description has been divided in three parts. In the first part, this article, we advance the realism of previous simulations by extending the model domain, by improving the representation of the surface and bottom boundary layers and the realism of the wind and tidal forcing, and by resolving the seasonal cycle. In forthcoming articles we will discuss the influence of density stratification and the interaction between the shelf and the deep-ocean circulations.

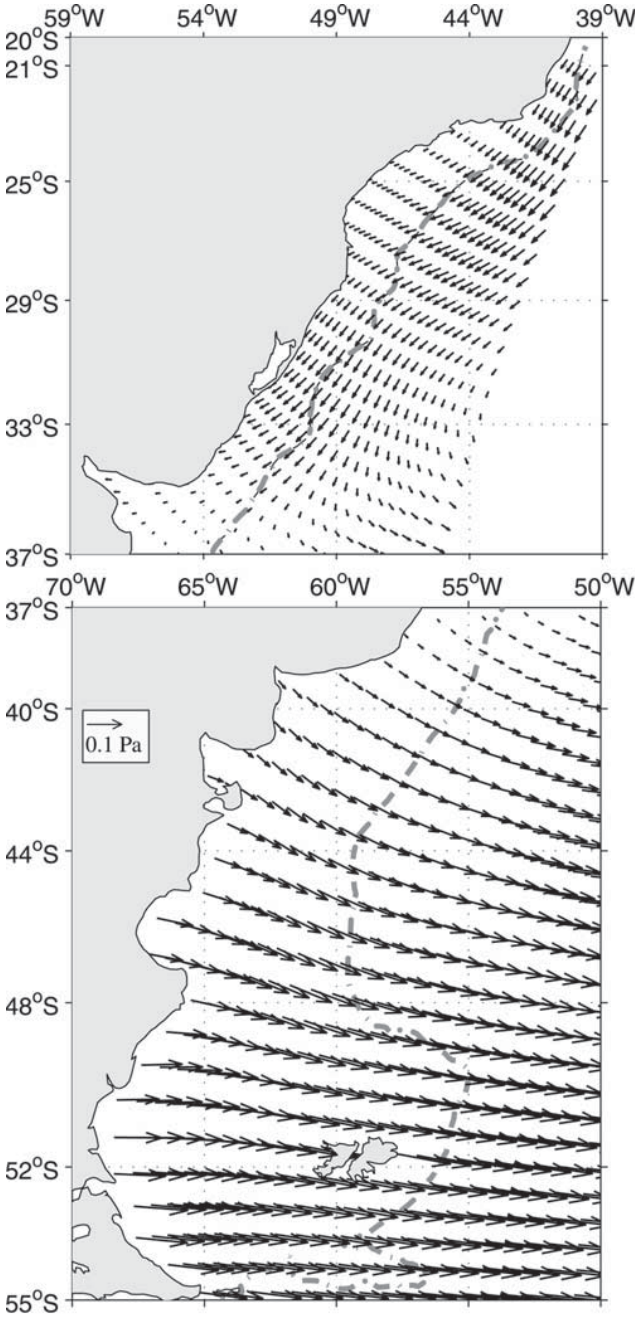

Figure 2. Annual mean wind stress distribution from *Trenberth et al.* [1990] interpolated onto the model domain. The dotted-dashed line indicates the 1000 m isobath.

[5] The layout of this article is as follows: After this introduction, in section 2, we review previous observational and numerical studies of the SWAS circulation. In section 3 we describe the model setup, and in sections 4 and 5 we describe and discuss the experimental results.

2. Background

[6] The range of tidal amplitudes in the SWAS grows from a few centimeters in the Brazilian sector to approximately 4.5 m at the southern end of the Argentinean Shelf [*Panella et al.*, 1991]. Current meter observations indicate that the tidal forcing accounts for more than 90% of the kinetic energy variance in the inner portion of the Patagonian Shelf ($z < 50$ m) and at least half of the variance of the outer shelf [*Rivas*, 1997]. Tides also affect the low-frequency variability through nonlinear tidal rectification and tidal mixing [*Glorioso and Simpson*, 1994]. *Glorioso and Flather* [1995, 1997] (hereinafter GF95 and GF97) using results from a barotropic model concluded that the inner shelf ($z < 100$ m) of the Patagonian region is largely dominated by the semidiurnal harmonic but that sea level variability in the outer shelf has equally significant contributions from the diurnal and semidiurnal tides. The tidal amplitudes in the region to the north of the Río de la Plata are significantly smaller than those in the Patagonian Shelf. *Zavialov et al.* [2002] analyzed a 6-month current meter record at a mooring site in the South Brazilian Shelf (34°S to 28.5°S) and concluded that the diurnal tides are more important than the semidiurnal tides. *Castro and Miranda* [1998], however, observed that in the South Brazil Bight (28.5°S to 23°S) the semidiurnal tides account for more than 50% of cross-shelf current variability.

[7] The wind stress distribution over the SWAS is characterized by relatively high mean values (~0.15 Pa) over the Patagonian Shelf and relatively low mean values (~0.05 Pa) farther north (Figure 2). Their magnitude and direction are modulated by the seasonal oscillations of the South Atlantic high-pressure system [*Höflich*, 1984]. Observations indicate that the wind stress forcing over the inner and middle Patagonian Shelf generates a northeastward mean flow (~4 cm/s) [*Rivas*, 1997]. Using a 1-D Ekman-type model, *Forbes and Garraffo* [1988] estimated surface currents with speeds of 20 cm/s and hypothesized that the northeastward transport peaks during the austral winter. GF95 used a barotropic 2-D model to investigate the annual mean over the Patagonian Shelf and observed the development of two wind-driven counterclockwise cells, one centered in the Grande Bay (~50°S) and the other in the San Jorge Gulf (~38°S). There are relatively fewer studies of the circulation in the northern region. *Pereira* [1989] hypothesized that the circulation over the South Brazilian Shelf reverses seasonally, but inverse calculations based on hydrographic data indicate that the middle shelf circulation is directed toward the northeast during the austral fall and only wanes in magnitude during the winter [*Zavialov et al.*, 2002]. Observations in the South Brazil Bight show the existence of a southwestward flow of approximately 0.5 m/s [*Castro and Miranda*, 1998].

3. Model Setup

[8] The numerical model used in this study is the Princeton Ocean Model (POM). The model equations, and the numerical algorithms used to solve them, have been described in detail by *Blumberg and Mellor* [1987]; therefore only a brief overview will be given here. The model solves the three-dimensional primitive equations on an Arakawa C grid. The numerical scheme conserves linear and quadratic quantities like mass and energy. The model uses sigma coordinates in the vertical and curvilinear coordinates in the horizontal. A Laplacian operator handles horizontal mixing in the model,

while the coefficients of vertical mixing are determined by a 2.5 turbulence closure scheme.

[9] The model domain extends from 55°S to 20°S and from 70°W to 40°W (Figure 1). The curvilinear horizontal grid has 250 grid points in the along-shelf direction, with an average resolution of 7.5 km, and 150 grid points in the cross-shelf direction, with an average resolution of 10 km. In the vertical the model equations are discretized in 25 sigma levels with small spacing at the top and the bottom to provide higher resolution of surface and bottom boundary layers. The barotropic simulation uses constant temperature (20°C) and salinity (35 practical salinity units). To improve the representation of the bottom relief over the shelf ($z < 250$ m), we dovetailed the *Smith and Sandwell* [1997] topographic data set with depths digitized from nautical charts provided by the Argentine Hydrographic Service. Regions with steep topographic gradients were smoothed to avoid the pressure gradient error associated with the sigma coordinate models [*Haney*, 1991].

[10] At the open boundaries we implemented the radiation conditions for the external and internal modes recommended by *Palma and Matano* [1998, 2000]. For the barotropic mode we used the condition proposed by *Flather* [1976], while for the internal velocities we used *Orlanski*'s [1976] radiation condition. The Flather radiation condition may be written in the form

$$U_n - U_n^o = \frac{c}{H}(\eta - \eta^o), \tag{1}$$

where g is gravity, H is the water depth, $c = \sqrt{gH}$ is the shallow water wave speed, and η^o and U_n^o are prescribed elevation and mean current normal to the boundary, respectively. In the experiments designed to investigate tidal circulation the sea surface elevation at the open boundaries (η^o) was taken from the values predicted by the global 0.5° resolution TPXO.5 Oregon State University (OSU) tidal model [*Egbert et al.*, 1994]. This model assimilates altimeter data collected by the TOPEX/Poseidon mission crossover and contains 10 major tidal constituents. The OSU model ranks among the top in its type, and it is superior to the *Schwiderski* [1980] model when compared with tidal gauges [*Andersen et al.*, 1995]. The unknown normal velocities at the open boundaries (U_n^o) were determined by an iterative procedure similar to that proposed by *Flather* [1987]. The simulations to be discussed did not include the effect of tidal potential because its overall effect is to change the solution by less than 2.5%.

[11] In some experiments the model was forced simultaneously by tides and surface wind stress values derived from the European Centre for Medium-Range Weather Forecasts (ECMWF) climatology compiled by *Trenberth et al.* [1990] (Figure 2). Previous modeling studies of this region used the *Hellerman and Rosenstein* [1983] winds, although recent articles have shown that in poorly sampled regions, like the Southern Hemisphere, this climatology underestimates the amplitude and seasonal variation of the wind stress [*Large and van Loon*, 1989; *Chelton et al.*, 1990].

4. Results

4.1. Tides

[12] Tides influence the magnitude of vertical mixing in regions of high amplitudes like the Patagonian Shelf. To account for their influence, our experiments were forced, at its open boundaries, with the M_2, S_2, N_2, K_1, and O_1 harmonics extracted from the Oregon State University model. Since the tidal-driven circulation over the southern and central portions of the SWAS has been well documented [e.g., *Glorioso and Simpson*, 1994; *Glorioso and Flather*, 1995, 1997; *O'Connor*, 1991] and the tidal-driven circulation in the northern portion of the SWAS has very small amplitudes, herein we only offer a succinct description of the tidal circulation derived from this simulation. The most important difference between this and previous simulations can be attributed to the use of a 3-D, sigma coordinate model with a turbulent closure scheme instead of a z level, 2-D model with constant mixing coefficients. The differences, however, are more quantitative than qualitative, and we will point them out in the ensuing discussion.

[13] The tidally driven simulation (no wind) can be characterized by the amplitude and phase of the principal harmonic (M_2), the tidal dissipation rate (that represents the magnitude of the residual currents), and the tidal energy fluxes. The M_2 harmonic is part of an amphidromic system located in the proximity of the Greenwich meridian and 60°S [*Genco et al.*, 1994]. It propagates from the southwest toward the northeast, and its amplitude decreases, because of frictional effects, from a maximum of 4 m in the Grande Bay to less than 30 cm north of Bahía Blanca (Figure 3a). Local maxima are observed in the San Matías Gulf, the Bahía Blanca Bay, and the head of the Río de la Plata estuary. The phase distribution over the Patagonian Shelf is characterized by amphidromes near 47°S 62°W, the San Blas Bay, and the south shore of the Malvinas Islands. The largest M_2 currents (not shown) are observed in the southern portion of the Patagonian Shelf with peak values larger than 1.5 m/s in regions of strong convergence (e.g., the Grande Bay). The K_1 currents are generally weaker than the M_2 currents, except in the southern portion of the outer shelf ($100 < z < 200$ m), where both harmonics have comparable amplitudes. The offshore intensification of the diurnal tidal currents has been attributed to their resonance with continental shelf waves [*Flather*, 1988; *Davies et al.*, 1997; *Han*,

Figure 3. (a) Cotidal charts of the main semidiurnal tidal constituent (M_2) derived from the model: amplitudes (color), contour interval (CI) = 25 cm, Greenwich phases (white solid lines), and CI = 20°. (b) Mean January sea surface temperature gradient (°C/100 km) determined from 12 years of satellite-derived SST data from 1987 to 1999 (data provided by A. Rivas). Only gradients larger than 2.5°C/100 km are shown. (c) Simpson-Hunter parameter [$\log(H/U^3)$] computed from the model results showing the location of the tidal shelf sea fronts. The 2.3-contour coincides with the location of the front northeast of Valdés Península as determined with satellite infrared images [*Glorioso and Simpson*, 1994] and is indicated as a heavy black line.

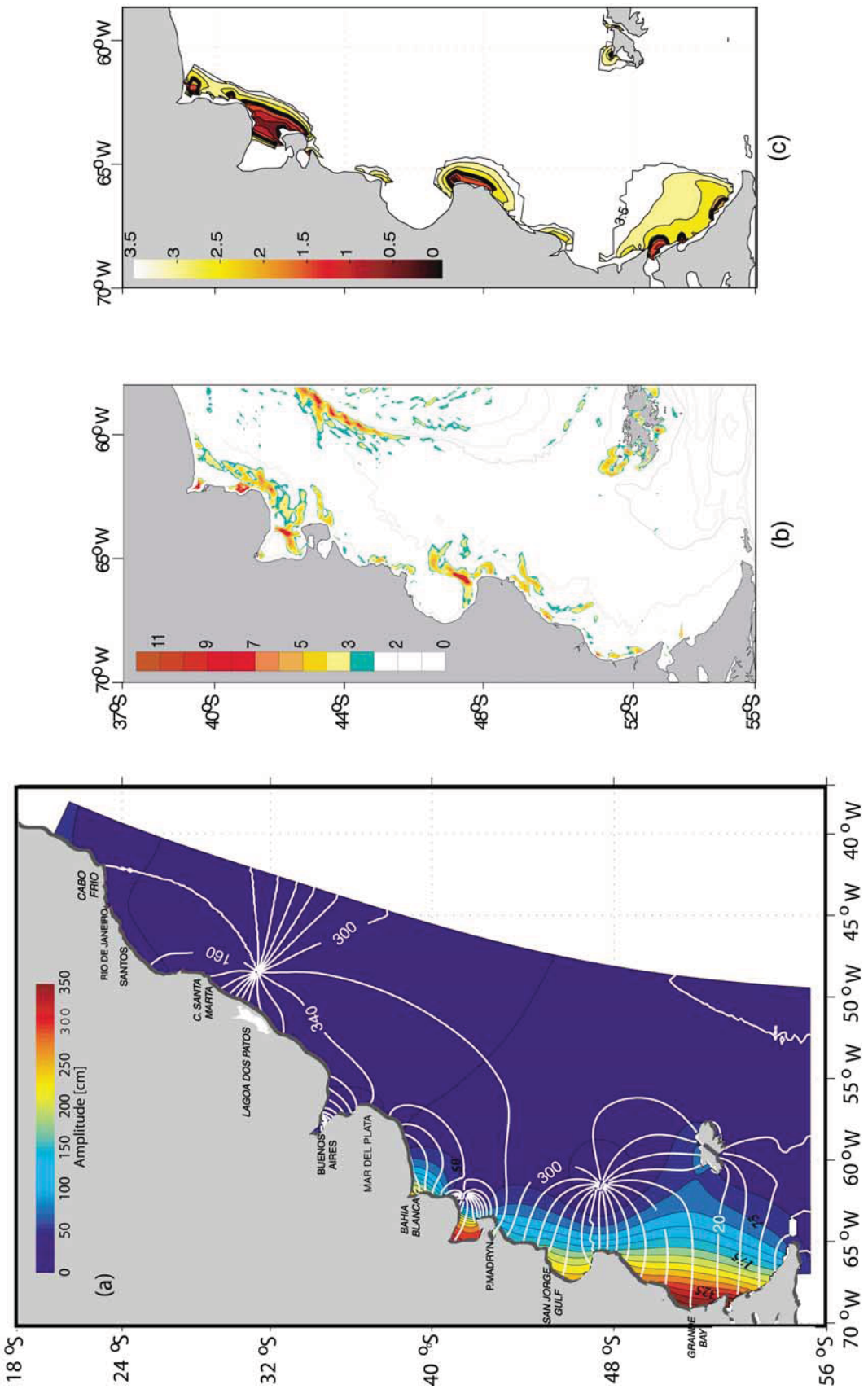
(a)
(b)
(c)
Amplitude [cm]
0 50 100 150 200 250 300 350
CABO FRIO
RIO DE JANEIRO
SANTOS
C. SANTA MARTA
LAGOA DOS PATOS
BUENOS AIRES
MAR DEL PLATA
BAHIA BLANCA
P.MADRYN
SAN JORGE GULF
GRANDE BAY
160
300
340
300
20
18 °S
24 °S
32 °S
40 °S
48 °S
56 °S
70 °W
65 °W
60 °W
55 °W
50 °W
45 °W
40 °W
37°S
40°S
44°S
48°S
52°S
55°S
70°W
65°W
60°W
11
9
7
5
3
2
0
3.5
3
2.5
2
1.5
1
0.5
0

Figure 3

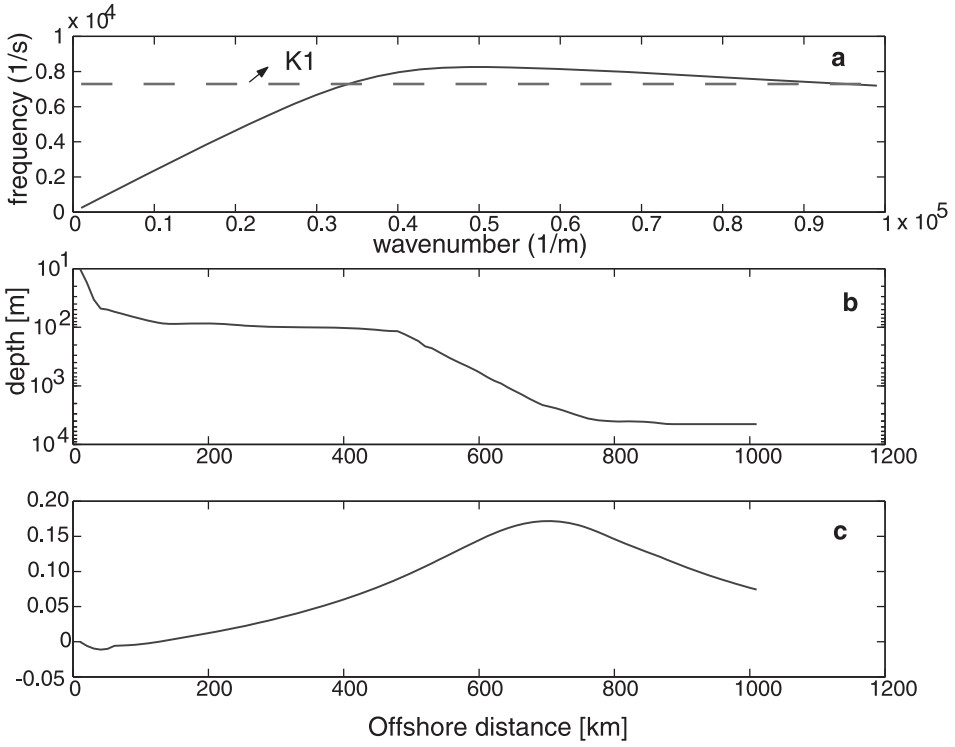

Figure 4. (a) Dispersion relation for the fist-mode continental shelf waves. The horizontal line indicates the K_1 frequency. (b) Bottom profile for the San Jorge Gulf section (Figure 1). Note the logarithmic vertical scale. (c) First eigenvalue of alongshore current speed for shelf waves at the K_1 frequency.

2000]. To investigate these matters, we computed the dispersion diagram for a section at 46°S (Figure 4) and found that the offshore increase in current speed observed in our simulation mimics the cross-shelf structure of the first-mode continental shelf wave at the K_1 frequency. The spatial and temporal structures of the S_2 and N_2 harmonics (not shown) are similar to the M_2 although with a substantially smaller amplitude. A calculation of the amplitude ratio $F = (M_2 + S_2)/(K_1 + O_1)$ indicates that the inner portion of the southern shelf is dominated by semidiurnal tides and that the outer portion and the northern shelf are dominated by mixed tides. The amplitudes and phases predicted by our simulation are in good agreement with previous modeling studies [*Genco et al.*, 1994; *Khanta*, 1995; *Le Provost et al.*, 1994; GF95; GF97].

[14] To illustrate the effects of the tidal residual circulation, we computed the Simpson-Hunter parameter (H/U^3) [*Sharples and Simpson*, 1996]. There is good agreement between model and observations (Figures 3b and 3c). The model, for example, correctly predicts the location of the main frontal systems of the Patagonian Shelf, i.e., the Valdés Península, Bahía Blanca, and Grande Bay [*Glorioso and Simpson*, 1994, GF97]. The M_2 energy flux over the SWAS is driven by the South Atlantic amphidrome [*Khanta*, 1995], which forces (in our simulation) 82 GW of tidal energy into the southern portion of the Patagonian Shelf that is dissipated by bottom friction (Figure 5). The dissipation is not uniformly distributed, but it is largely concentrated in the shallow regions of the northern portion of the Patagonia Shelf. According to this simulation the M_2 harmonic dissipates 110 GW of astronomical energy. This value is in good agreement with the 115 GW average estimated by *Egbert and Ray* [2001], but it is smaller than the 220 GW and 245 GW estimated by GF97. These differences can be ascribed to differences in the method of calculating the dissipation rates. In this article we use bottom velocities, while GF97 used depth-averaged velocities. This simulation also differs from the early study of GF97 in the parameterization of vertical mixing; our model has embedded a turbulent closure scheme for calculation of the bottom boundary layer flow, while GF97 used a constant bottom friction coefficient.

4.2. Wind Forcing

4.2.1. Annual Mean Circulation

[15] To estimate the mean, wind-driven circulation over the SWAS, we forced the model with the ECMWF winds [*Trenberth et al.*, 1990] (Figure 2). This simulation also includes tidal forcing to account for the effect of tidal-induced mixing. The experiments were started from rest and spun up to barotropic equilibrium. The spin-up period is relatively short (~5 days). For the purposes of the analysis, however, we integrated our simulations for a 90-day period and saved the last 30 days of numerical integration for the analysis. To separate the wind from the tidal circulation, we subtracted from this simulation the tidal currents obtained from the tidal simulation described in section 4.1.

[16] The westerly winds over the Patagonian Shelf force an intense offshore flow composed of a geostrophic and an Ekman component. Close to shore, in areas of large surface depressions (Figure 6b), the surface currents are aligned

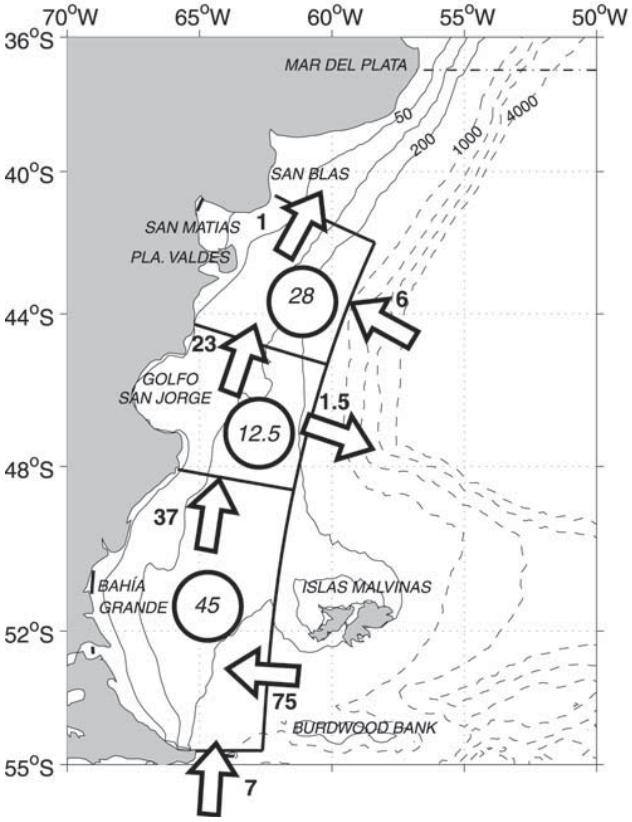

Figure 5. Tidal energy fluxes in Gigawatts (arrows) and tidal energy dissipation (circles) for the Patagonian shelf. Solid lines indicate the 50-, 100-, and 200-m isobaths, and dashed lines indicate the 1000-, 2000-, 3000-, and 4000-m isobaths.

with the wind. Farther offshore, away from boundary influences, the currents veer to the left of the wind as expected from Ekman dynamics (Figure 6a). The depth-averaged circulation in the middle and outer shelf consists of a broad, northward flow that branches north of the Grande Bay (Figure 6c). This circulation pattern is qualitatively similar to that inferred from hydrographic observations and zooplankton distribution by *Sabatini et al.* [2004]. The northward volume transport varies from 0.66 Sv at 51°S to less than 0.1 Sv north of 44°S. The northward Ekman transport over the Patagonian Shelf is sustained by a southward flow in the bottom boundary layer and a widespread upwelling (Figure 6d). The most conspicuous features of this region are the recirculation gyres in the Grande Bay and the San Jorge Gulf (Figure 6c). North of 40°S, there is a sea level set down, associated with the predominantly northeasterly winds (Figure 7b), and a geostrophically balanced southward coastal jet (Figure 7a). The volume transport in this region varies from a maximum of 0.45 Sv at 25°S to a minimum of 0.05 Sv at 35°S. The southward flow from the northern shelf and the northward flow from the southern shelf collide near the mouth of the Río de la Plata and turn offshore (Figure 7c). In the bottom layer (Figure 7d) the frictional turning of the near-bottom velocities down the pressure gradients results in cross-isobath flows and upwelling in several coastal locations (i.e., southern Uruguay, Santos Bay, and Cabo Frío).

[17] There are significant differences in the vertical structures of the currents in the northern and southern portions of the shelf. In the north the currents have a nearly uniform vertical structure, while in the south the currents are strongly confined to uppermost layers of the water column (Figure 8). In the northern region the predominantly alongshore wind forcing, and the relatively narrow span between the coast and shelf break, allows the development of significant pressure gradients and an associated geostrophic flow (Figure 8a). In the southern region, however, and far from coastlines irregularities, the relatively wide span of the shelf and the predominately offshore direction of the wind forcing limits the development of significant cross-shore pressure gradients, and the circulation is largely confined to a frictional, top Ekman layer (Figure 8b).

[18] To gain further understanding of the dynamics of the circulation, we did a momentum and vorticity balance of the model results. The momentum equation for the steady flow is

$$[-\mathbf{k}\cdot(f\mathbf{V}D)] - [gD\nabla\eta] + \left[\frac{1}{D}(-\mathrm{ADV}+\mathrm{DIFF})\right] + \left[\frac{\boldsymbol{\tau}^{\mathbf{w}}}{D}\right] - \left[\frac{\boldsymbol{\tau}^{b}}{D}\right] = 0, \quad (2)$$

where f is the Coriolis parameter, $\mathbf{k}$ is the vertical unit vector, $\mathbf{V}$ is the horizontal velocity vector, D is the water depth, η is the surface elevation, ADV is the horizontal component of advection, DIFF is the horizontal component of diffusion, $\boldsymbol{\tau}^{w}$ is the wind stress vector, and $\boldsymbol{\tau}_b$ is the bottom stress. The square bracketed momentum terms in equation (2) are hereinafter identified as Coriolis, elevation gradient, advection (plus diffusion), wind stress, and bottom stress.

[19] The relative contribution of the geostrophic and frictional effects to the SWAS circulation varies with latitude and the offshore distance (Figures 9 and 10). These variations are caused by changes in the shelf width, the shape of the bottom, and the relative influence of the atmospheric and tidal forcing. The southern portion of the SWAS, for example, has a wide span, and it is forced by strong, offshore winds and large tidal amplitudes, while the northern portion is relatively narrow, the tidal amplitudes are very small, and it is forced by weak, alongshore winds.

[20] There are three distinct dynamical regimes in the southern region (Figure 9). In the inner shelf, i.e., from the coast to approximately 120 km, the circulation is characterized by a northeastward flow in the upper portion of the water column and an opposite, southwestward flow farther down (Figure 8a). The momentum balance in this region is partitioned between the Ekman balance of the upper flow (wind stress and the Coriolis term) and the geostrophic balance of the deeper flow (Coriolis and elevation gradient). The deep flow is part of the Grande Bay recirculation cell described previously (Figure 6c). The cross-shore momentum balance indicates that this cell is driven by the coastal sea level gradient generated by the offshore component of the wind stress (the alongshore winds are very small at these

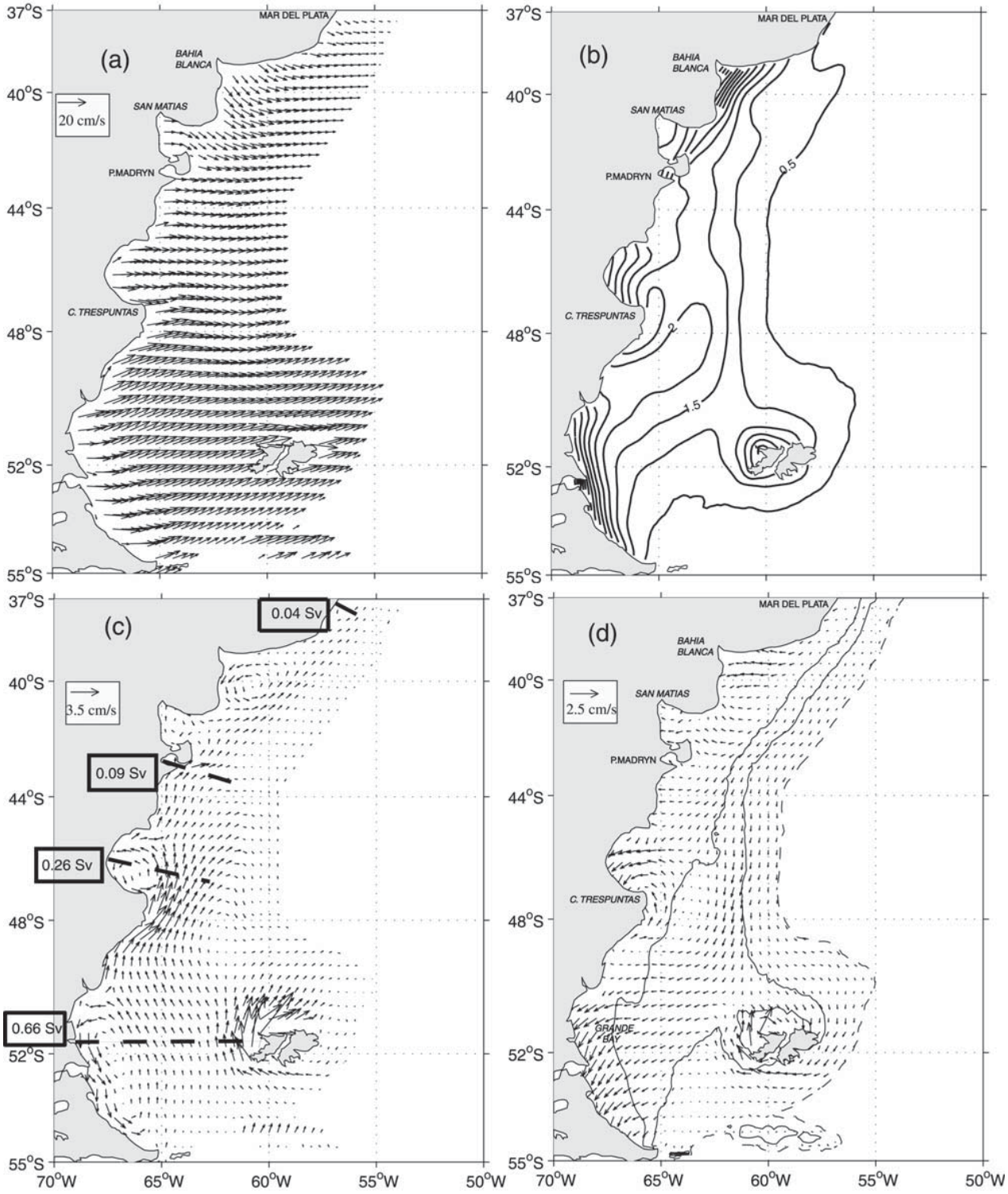

Figure 6. Model results from the experiment forced by annual mean wind stress (Patagonian Shelf). (a) Surface velocities. (b) Surface elevation. Solid lines indicate negative values (CI = 0.5 cm). (c) Depth-averaged velocity vectors (numbers inside boxes indicate the transport in sverdrups through the indicated cross section). (d) Near-bottom velocity vectors. Solid lines indicate the 100- and 200-m isobaths; the dashed line is the 1000-m isobath. The fields are shown for depths of less than 1000 m.

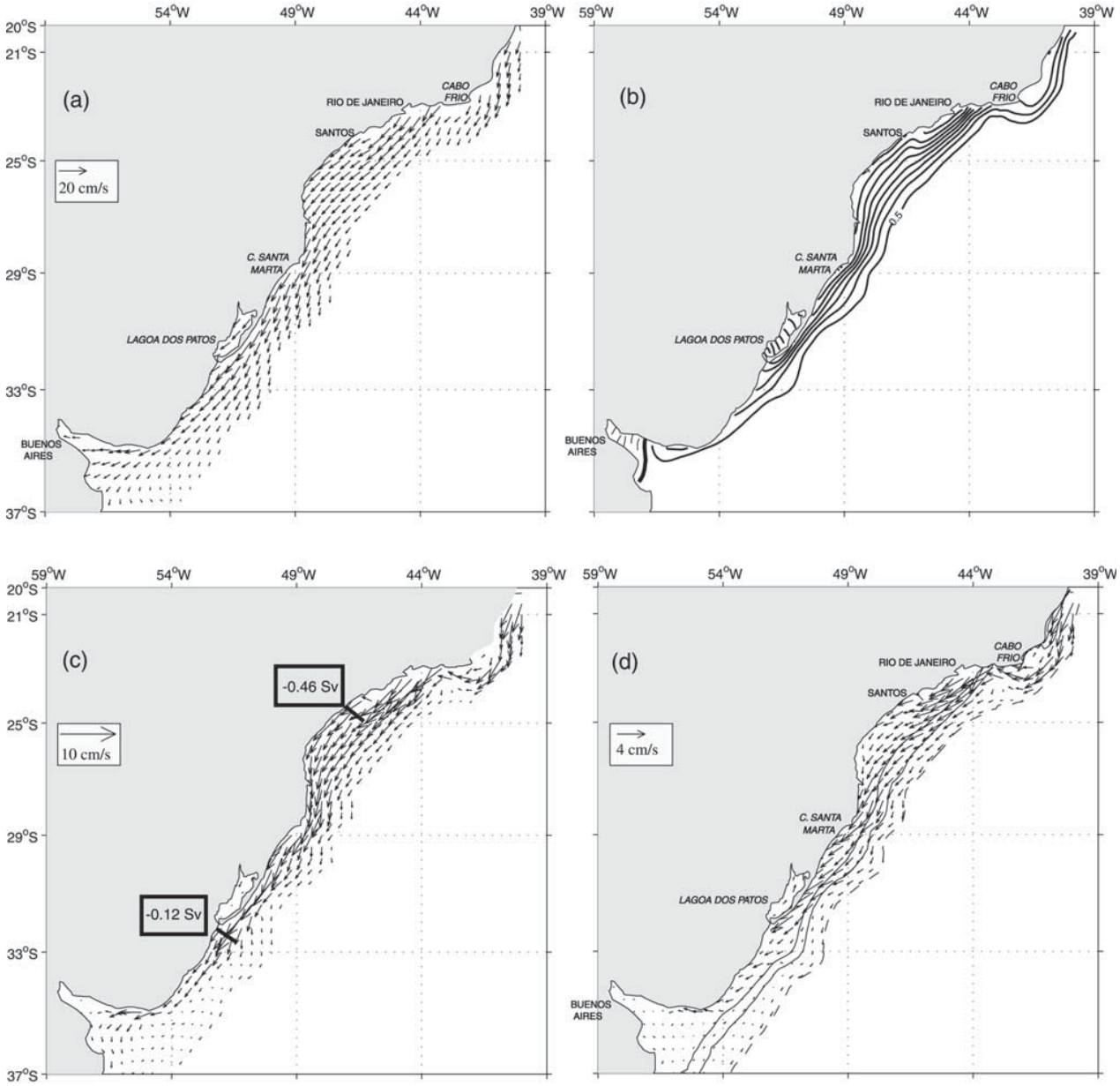

Figure 7. Model results from the experiment forced by annual mean wind stress (northern shelf). (a) Surface velocities. (b) Surface elevation. Solid lines indicates negative values (CI = 0.5 cm). (c) Depth-averaged velocity vectors (numbers inside boxes indicate the transport in sverdrups through the indicated cross section). (d) Near-bottom velocity vectors. Solid lines indicate the 100- and 200-m isobaths; the dashed line is the 1000-m isobath. The fields are shown for depths of less than 1000 m.

latitudes) (Figure 9a). Farther from the coast, the circulation is in Ekman balance, except near the Malvinas Islands, where the shelf break allows the development of significant pressure gradients that lead to the development of a strong coastal jet. The terms of the momentum balances of the alongshore circulation are significantly smaller than those corresponding to the cross-shore circulation (Figure 9b). In the inner shelf the contribution from the bottom stress increases because of the predominately alongshore direction of the circulation. The meridional currents over the middle shelf are primarily in geostrophic balance.

[21] North of approximately 33°S, there is a rapid transition from the broad shelf and highly irregular coasts of Patagonia to a more narrow shelf bounded by a relatively smooth coastline. In this region, there is also a transition from the strong, offshore winds characteristic of the southern domain toward relatively weak, along-shelf winds (Figure 2). The momentum balance of this region is typified by a cross section near the Lagoa dos Patos (Figure 10). There, the alongshore wind stress generates a cross-shore pressure gradient that is compensated by a quasi-geostrophic current (Figure 10a). The

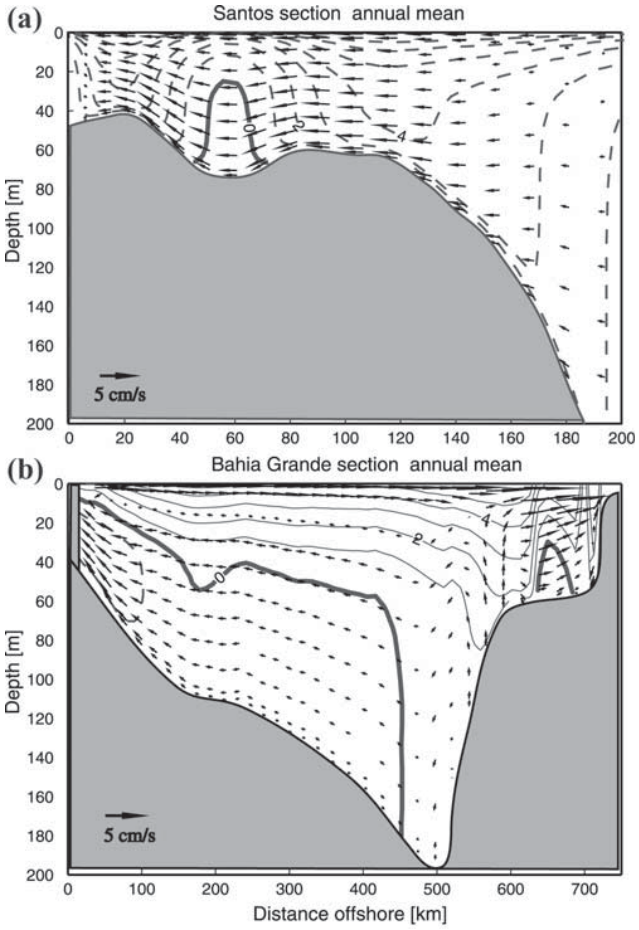

Figure 8. Cross sections showing isotachs of normal velocity (cm/s) and tangential velocity vectors. (a) Santos section. (b) Grande Bay section. Dashed lines indicates negative (i.e., southward) velocity. The location of the cross sections is indicated in Figure 1. Note that the panels have different horizontal scales.

alongshore momentum balance, however, is essentially dominated by Ekman dynamics (Figure 10b).

[22] Further understanding of the shelf dynamics can be gained from the vorticity balance, i.e.,

$$-D\left[\mathbf{V}\cdot\nabla\left(\frac{f}{D}\right)\right]+\mathrm{curlz}\left[\frac{1}{D}(-\mathrm{ADV}+\mathrm{DIFF})\right]+\mathrm{curlz}\left[\frac{\boldsymbol{\tau}^{\mathbf{w}}}{D}\right]-\mathrm{curlz}\left[\frac{\boldsymbol{\tau}^{\mathbf{b}}}{D}\right]=0, \quad (3)$$

where the four terms in equation (3) are stretching (includes the Beta effect), advection (the curl of advection plus diffusion), the wind stress curl, and the bottom stress curl.

[23] The vorticity balance of the southern region is primarily driven by a vorticity input from the wind stress curl, which is compensated by vortex stretching or by advection and bottom friction (Figure 11). Vortex stretching is the dominant mode of ocean adjustment in the deep portions of the shelf (Figure 11b), while advection and friction dominate in the shallow, nearshore regions (Figures 11c and 11d). The regions where the vorticity input by the wind is compensated by vortex stretching are prone to upwelling or downwelling and, consequently, cross-isobath flows. Our experiment also indicates that the intensity of these cross-isobath flows is highly dependent on the tidal-induced mixing. In fact, in experiments without tidal forcing (not shown) the contribution from the bottom friction terms to the vorticity (and momentum) balance decreased by almost an order of magnitude. This decrease was largely compensated by an increase of vortex stretching (with only relatively minor changes in the magnitude of the advection term). Our results therefore indicate that tidal mixing tends to arrest cross-isobath flows by increasing the magnitude of the bottom friction.

[24] Unlike the southern region, where the vorticity balance is largely driven by the wind forcing, in the northern region vorticity advection plays an equally important role (Figure 12). The difference between both regions can be ascribed to the differences in the shelf width. In the northern region the narrower shelf and larger depth gradients generates a larger component of cross-isobath flow

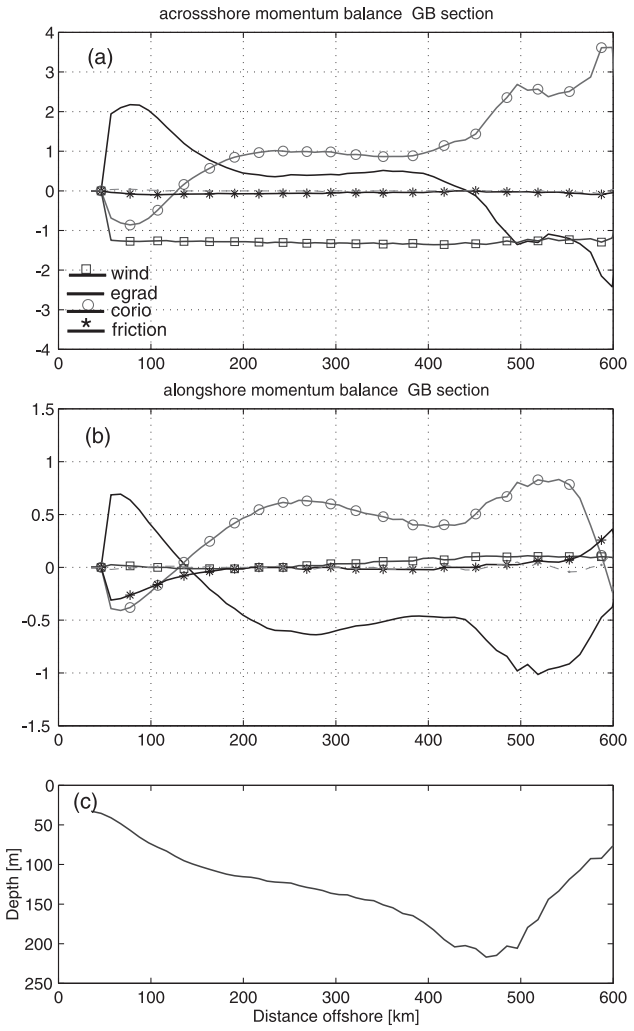

Figure 9. (a) Across-shore depth-integrated momentum terms sampled offshore Grande Bay. Units are 10^{-4} m^2/s^2. (b) Alongshore momentum terms. (c) Bottom topography.

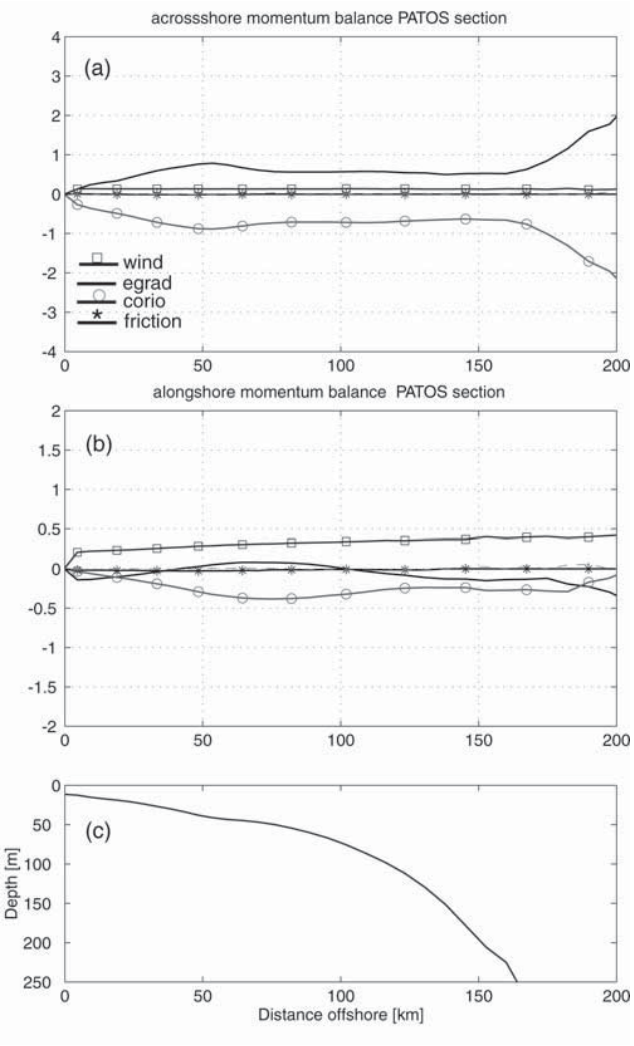

Figure 10. (a) Across-shore depth-integrated momentum terms sampled offshore Lagoa dos Patos. Units are 10^{-4} m^2/s^2. (b) Alongshore momentum terms. (c) Bottom topography.

that, in the absence of significant bottom friction, can only be compensated by vortex stretching. The wind forcing near Cabo Santa Marta (~27°S), for example, triggers the generation of shelf waves (reflected by the balance between stretching and advection observed in Figures 12b and 12c, respectively), which propagate upstream. The combination between northward propagating waves and the southward mean flow leads to the formation of the stationary wavelike patterns observed in Figure 12b. To confirm this hypothesis, we did an additional experiment forced by northeastward winds [*Hellerman and Rosenstein*, 1983], and in that case the stationary wave pattern disappeared.

[25] The circulation patterns predicted by the model over the southern shelf are in general agreement with hydrographic observations [e.g., *Boltovskoy*, 1981; *Bakum and Parrish*, 1991; *Guerrero and Piola*, 1997]. The observations, however, are sparse and cannot be used to corroborate the model details. Given the lack of observational evidence, it seems a useful exercise to compare the model results with previous simulations. *Forbes and Garraffo* [1988] and GF95 diagnosed a northward current, mostly trapped between the 100- and 200-m isobaths whose transport increased to the north. The present simulation, however, indicates that the bulk of the northward transport is concentrated inshore of the 100-m isobath, that it does not increase to the north, and that it has smaller magnitudes than those suggested by *Forbes and Garraffo* [1988] and GF95. We found, through the execution of an additional experiment forced with the *Hellerman and Rosenstein* [1983] climatology, that the differences between simulations are mostly due to the differences in the wind climatologies used to force the models (E. D. Palma et al., manuscript in preparation, 2004). *Forbes and Garraffo* [1988] and GF95 used the older *Hellerman and Rosenstein* [1983] climatology, while our simulation uses the relatively more realistic ECMWF wind stress distribution. Although the lack of observations does not allow us to determine which of these simulations is more realistic, the recent hydrographic analysis of *Sabatini et al.* [2004] suggests the existence of a circulation pattern in the southern Patagonian Shelf that is in close agreement with the one predicted by the model, specifically, a broad northward flow from Tierra del Fuego up to Cabo Tres Puntas where the northward flow turns offshore (Figure 6c), instead of the predominantly northward pattern predicted by the previous studies.

4.2.2. Seasonal Cycle

[26] The seasonal changes of the wind stress forcing over the SWAS are largely determined by the meridional displacements of the South Atlantic high-pressure center [*Höflich*, 1984]. South of 45°S, the wind stress is predominantly offshore throughout the year, being strongest during the fall and weakest during the spring (Figures 13a and 13b, bottom panels). Farther north, the largest seasonal variations of the wind stress distribution occur in the region between 37°S and 27°S where the wind veers from a NNW direction during the fall to a NNE direction during the spring (Figures 13a and 13b, top panels). On the basis of this wind distribution, earlier modeling studies of the shelf circulation suggested that this region shows the largest seasonal variations of the continental shelf [*Pereira*, 1989; *Lima et al.*, 1996]. There are, however, only scant data to characterize the seasonal changes of the shelf circulation. Hydrographic observations, for example, indicate that the freshwater plume associated with the discharges of the Rio de la Plata extends farther north during the winter than during the summer. Since the Rio de la Plata discharge has no significant seasonal variations, these changes have been attributed to changes in the wind-driven circulation [*Piola et al.*, 2000].

[27] To investigate the seasonal evolution of the wind-driven circulation, we run an additional experiment forced with the monthly wind climatology of *Trenberth et al.* [1990]. The mean circulation corresponding to the two most contrasting seasons (fall and spring) is displayed in Figure 14, which shows a general strengthening of the northward circulation during the fall and a weakening during the spring. In the southern portion of the shelf, there is weakening of the northward, inner-shelf jet during the spring and a reversal of the outer-shelf circulation from a southward direction during the fall toward a northward direction during the spring. There are no significant seasonal variations of the wind-driven circulation south of

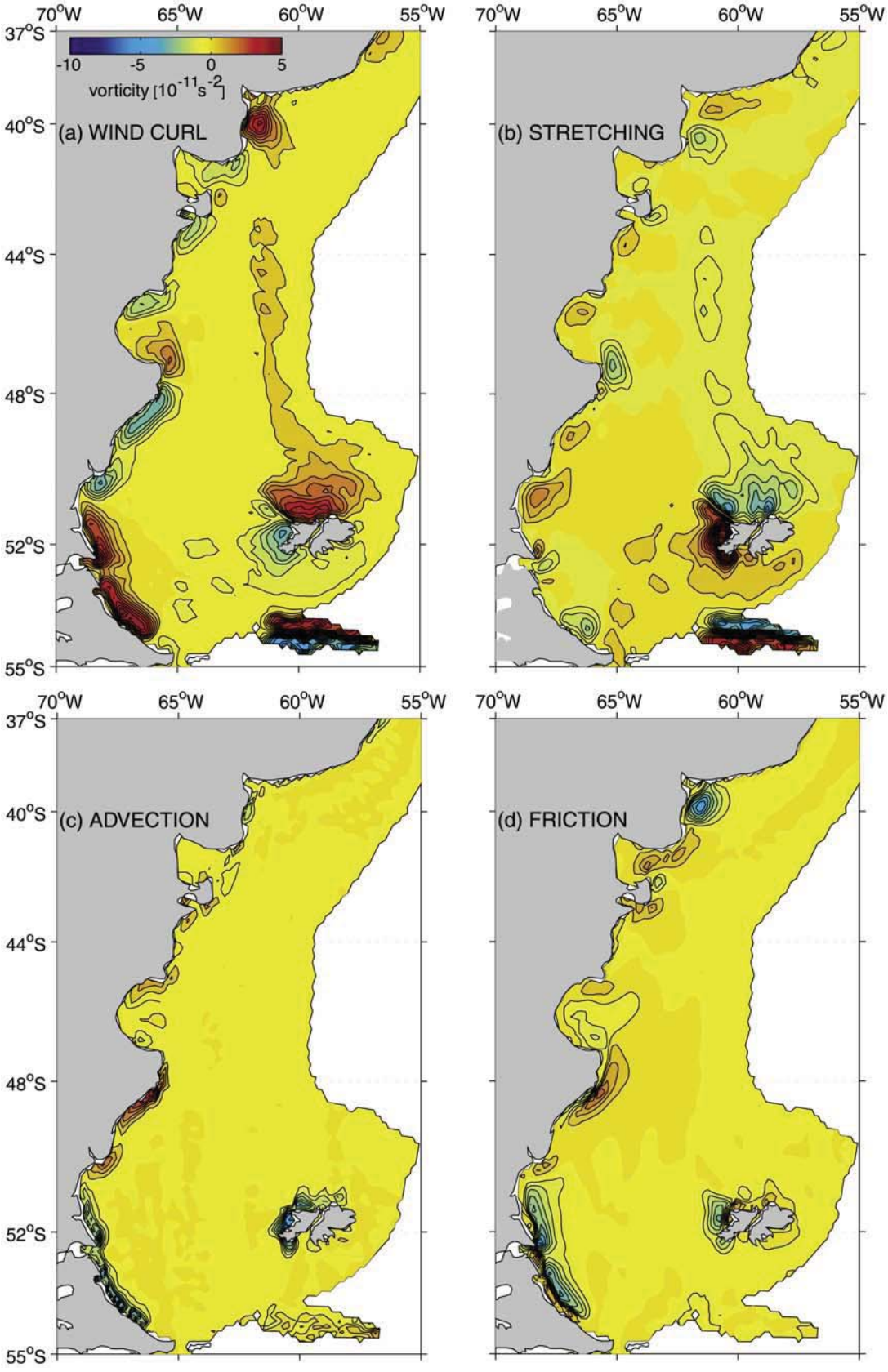

Figure 11. Maps of time-averaged external mode contributions to the vorticity balance (Patagonian Shelf). (a) Wind stress curl. (b) Stretching. (c) Advection plus diffusion. (d) Bottom stress curl. Contour interval is 0.5×10^{-12} s^{-2}.

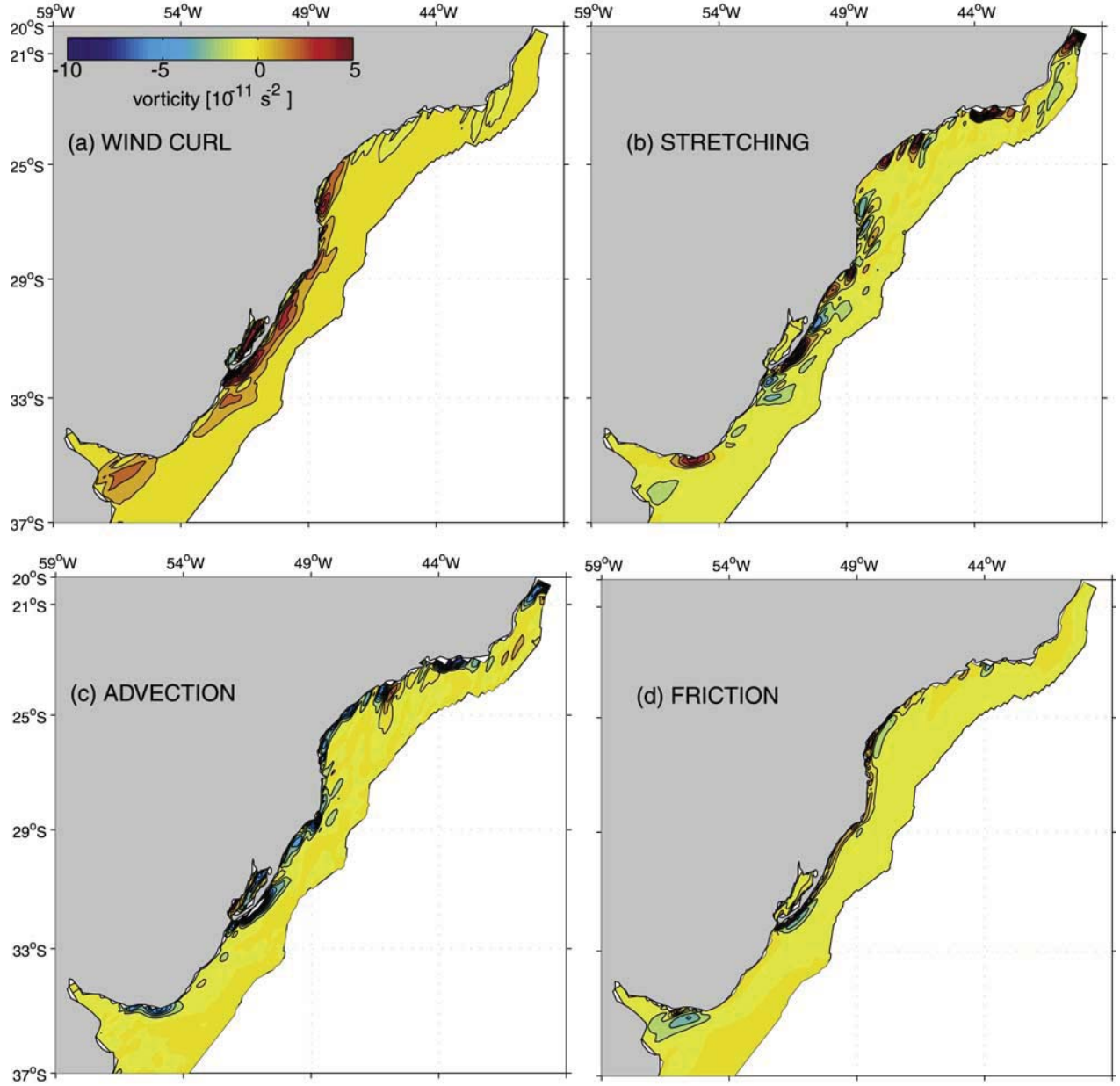

Figure 12. Maps of time-averaged external mode contributions to the vorticity balance (northern shelf). (a) Wind stress curl. (b) Stretching. (c) Advection plus diffusion. (d) Bottom stress curl. Contour interval is 0.5×10^{-12} s^{-2}.

~50°S. The largest seasonal variations are observed in the central and northern portion of the shelf. Near Mar del Plata (~38°S), for example, there is a reversal of the coastal jet that hugs the continental boundary from a northward direction during the fall to a southward direction during the spring (Figures 15a and 15d). The abrupt change of the flow direction predicted by the model has been reported in hydrographic [*Martos and Piccolo*, 1988] and biological studies [*Carreto et al.*, 1995]. A similar phenomenon occurs in the South Brazilian Shelf (offshore of the Lagoa dos Patos, Figures 15b and 15e). The changes predicted by the model were also forecasted in the modeling study of *Pereira* [1989] and diagnosed in the observational study of *Lima et al.* [1996]. *Castro and Miranda* [1998] observed significant seasonal variations of temperature and salinity in the South Brazilian Shelf. These observations indicate the existence of a northward flow that can reach up to 30.5°S during the austral winter; such a circulation pattern is consistent with the model results (Figure 14a). Farther north, the surface currents reach a peak of 30 cm/s during the spring and weaken toward the fall. In the upwelling region of Cabo Frio (Figures 15c and 15f), the onshore velocities during the fall are weak, but during the spring the strengthening of the onshore flow, with the coastal jet reaching 10 cm/s, strengthens the upwelling activity. Although there are only scant in situ observations to compare, the circulation pat-

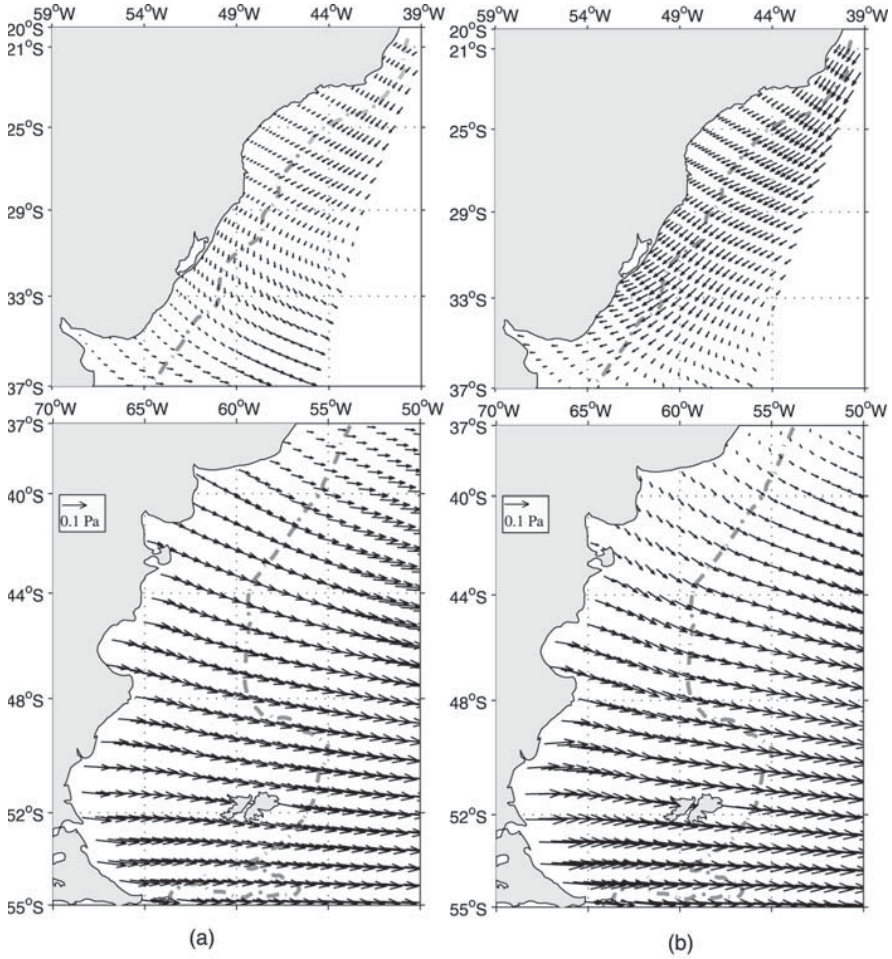

Figure 13. The climatological wind stress distribution from *Trenberth et al.* [1990] interpolated onto the model grid. (a) Fall season. (b) Spring season. The dotted-dashed line indicates the 1000-m isobath.

terns predicted by the model are in agreement with the circulation inferred from current meter records in the South Brazil Bight [*Castro and Miranda*, 1998] and regional models of the Cabo Frío upwelling regime [*Rodrigues and Lorenzetti*, 2001].

5. Summary and Conclusions

[28] This article discusses the results of a barotropic simulation of the SWAS circulation forced with tides and winds. The tidal experiments show the dominance of the semidiurnal harmonic in the southern portion of the shelf, particularly over shallow regions of the Patagonian Shelf. The tidal currents associated with the diurnal harmonic are generally weak except in some regions of the outer shelf and the shelf break zone because of their resonance with a first-mode shelf-trapped wave. Although there are only scant in situ observations to compare the model with, there is general agreement between the M_2 currents predicted by the model and those determined from current meter observations. The nonlinear interaction between the tidal currents and the bottom topography in the model leads to the formation of tidal fronts near the Valdés Península, the San Jorge Gulf, and the Grande Bay. The location of these fronts corresponds with the locations determined from satellite imagery [*Glorioso and Simpson*, 1994]. The tidal energy balance indicates that the bulk of the dissipation (~110 GW) occurs south of 40°S.

[29] There is a marked contrast in the characteristics of the wind-driven circulation of the northern and southern shelves. The offshore winds over the southern region generate a general depression of the coastal sea level and a northeastward flow. Coastline indentations (e.g., the Grande Bay and at the San Jorge Gulf) lead to the formation of quasi-stationary (counterclockwise) gyres and boundary currents. In the northern shelf, there is a southwestward flow that is geostrophically driven by the northeasterly winds. Although the magnitude of these winds is significantly smaller than those in the south, their influence on the circulation is amplified by the narrow span of the shelf region.

[30] The largest seasonal variations of the wind-driven circulation are observed north of 45°S. During the fall, there is a clockwise gyre over the middle Patagonian Shelf and a northward flowing coastal jet that extends as far as 29°S (Figures 14a and 14b). During the austral spring, there is a relaxation of the Patagonian gyre and the formation of a southward coastal flow that extends from Cabo Frío to Bahía Blanca (Figures 14c and 14d). At this time, there is active upwelling along the Brazilian coast. According to the results discussed herein, there are significant dynamical

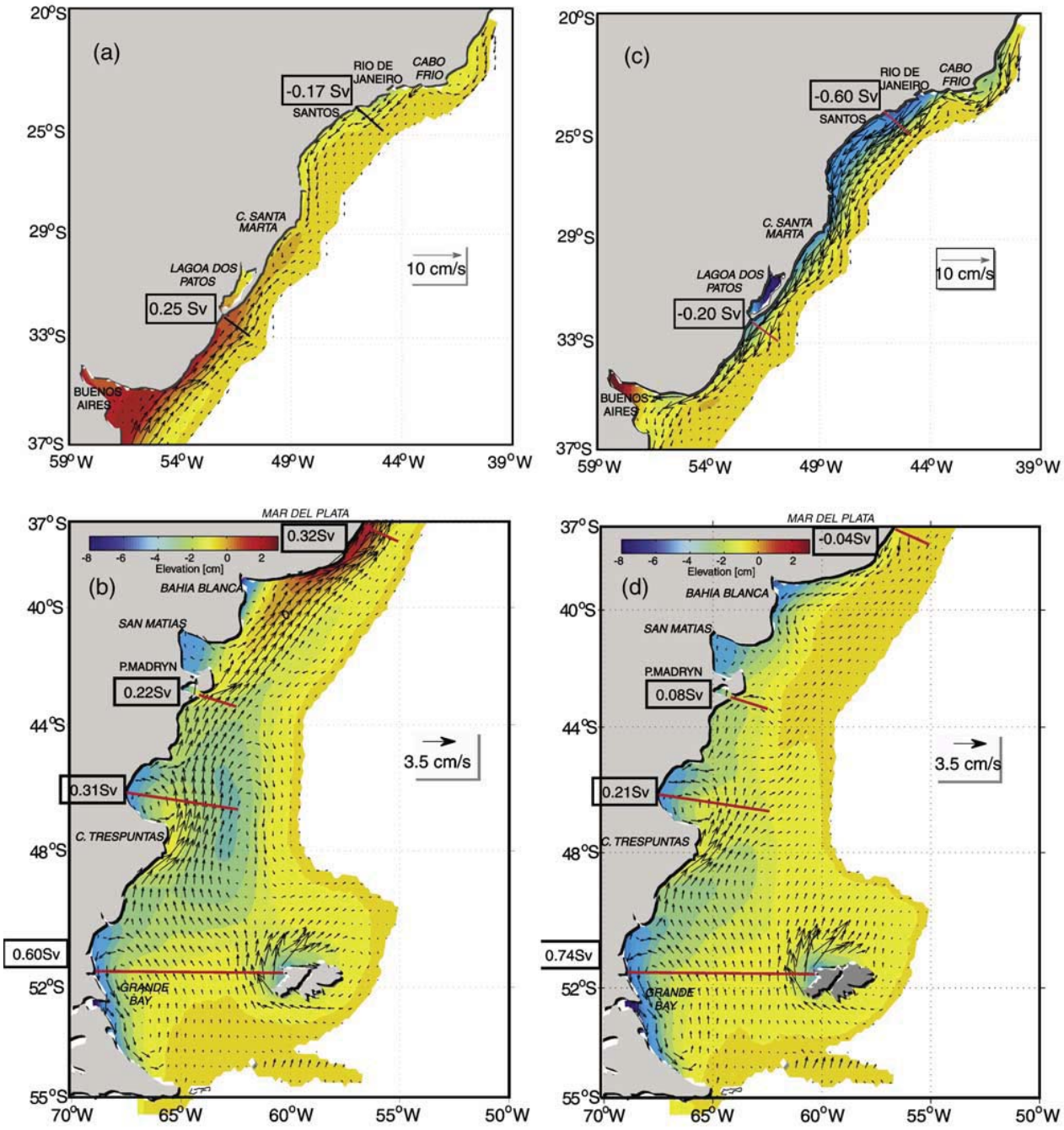

Figure 14. Sea surface elevation (solid contours, CI = 0.5 cm) and depth-averaged currents from the model simulation forced by climatological monthly winds. (left) Results for the fall season: (a) northern shelf and (b) Patagonian Shelf. (right) Results for the spring season: (c) northern shelf and (d) Patagonian Shelf. Numbers inside boxes indicate transport through the indicated cross section. The fields are plotted for depths of less than 1000 m.

connections between the circulations of the northern and southern shelves. Relatively cold and fresh waters from southern Patagonia can be brought in close contact with the warmer and saline waters of the Brazilian Shelf during fall and, conversely, during spring.

[31] The lack of long-term current meter observations across the shelf region does not allow us to verify the magnitude of the northward transport over the middle Patagonian Shelf nor the existence of counterclockwise gyre patterns in the inner shelf, although our results appear to be consistent with the circulation patterns derived from historical hydrographic and biological data [e.g., *Boltovskoy*, 1981; *Bakum and Parrish*, 1991; *Guerrero and Piola*, 1997; *Sabatini et al.*, 2004]. The seasonal cycles of flow reversals in the inner shelf between 42°S and 28°S derived from our numerical experiments appear to be

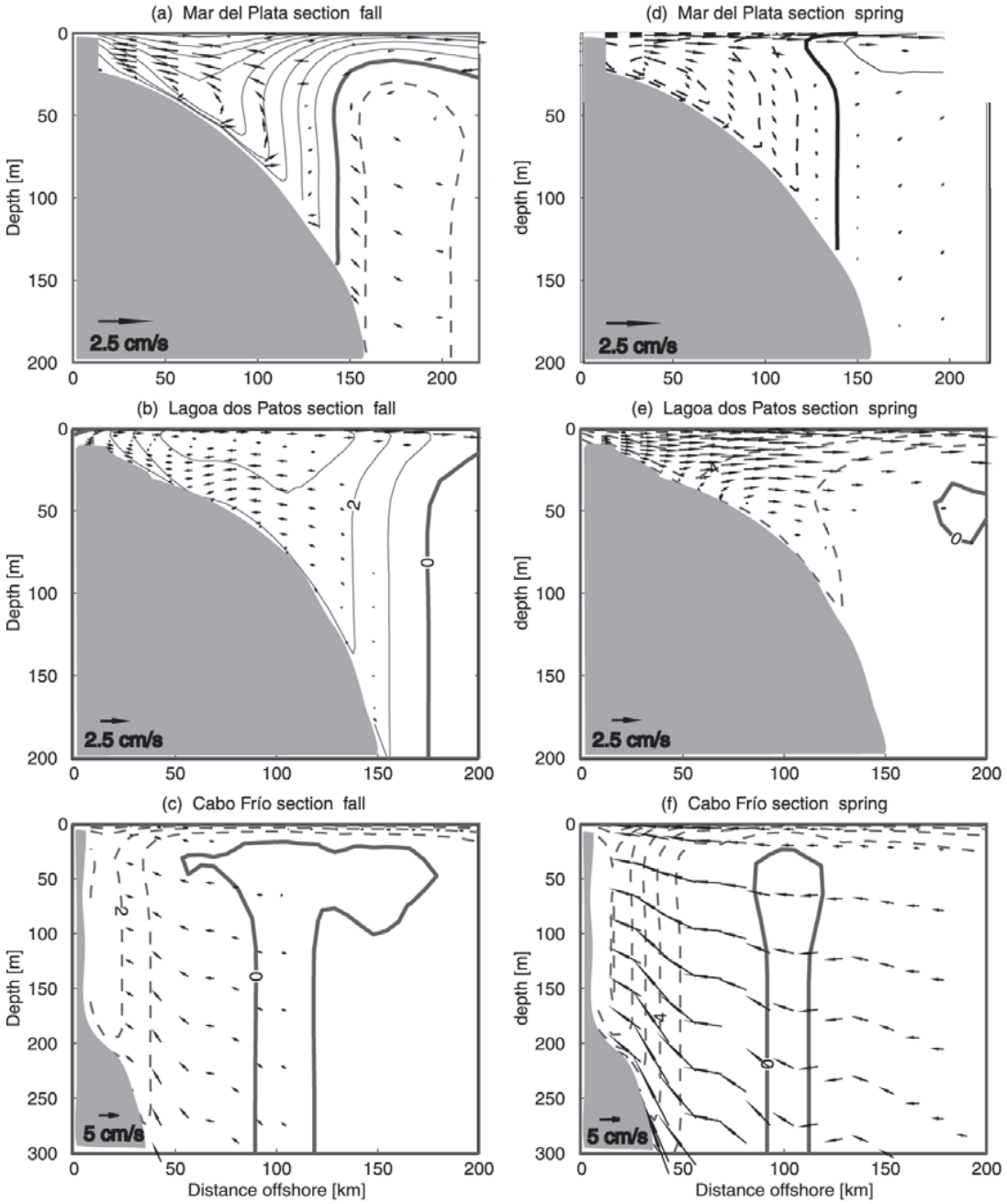

Figure 15. Cross sections showing isotachs of normal velocity (cm/s) and tangential velocity vectors in (left) fall for (a) Mar del Plata, (b) Lagoa dos Patos, and (c) Cabo Frío sections and (right) spring for (d) Mar del Plata, (e) Lagoa dos Patos, and (f) Cabo Frío sections from the model simulation forced by climatological monthly winds. Dashed lines indicate negative (i.e., southward) velocity. The location of the cross sections is indicated in Figure 1.

consistent with hydrographic observations and property distributions [*Martos and Piccolo*, 1988; *Carreto et al.*, 1995; *Lima et al.*, 1996; *Piola et al.*, 2000], which indicates a strengthening of the southwestward coastal circulation during spring and the formation of northeastward flow during fall. Farther north, in the South Brazil Bight, the model-predicted currents flow predominantly to the southwest during the whole year, being more intense during spring than during fall, a result that is qualitatively consistent with measurements and previous small-scale numerical models [*Castro and Miranda*, 1998]. Coastal sea level studies conducted in the South Brazil Bight also show seasonal variations, with high values during autumn-winter and low values during spring-summer, a result in accordance with the model-predicted sea level changes (Figures 14a and 14c). In spite of the above agreements it should be noted that the circulation scheme described above is an initial step aimed at understanding the full three-dimensional

circulation of the SWAS. Climatological wind stress forcing alone cannot account for the observed seasonal variability of the shelf circulation. Contributions of barotropic inflows from the Malvinas Current to the circulation over the upper Patagonian continental slope and penetrations of the Brazil Current on the Brazilian Shelf are quite possible. It is also possible that the variability of the Brazil-Malvinas Confluence induces spatial and temporal fluctuations on the shelf circulation. A more quantitative study of the SWAS circulation with the incorporation of boundary inflows and freshwater forcing will be the subject of forthcoming studies.

[32] **Acknowledgments.** Support for E. D. Palma and A. R. Piola came from Agencia Nacional de Promoción Científica y Tecnológica (ANCYPT) through grant PICT99-0706420. E. D. P. was partially supported by Universidad Nacional del Sur (Argentina). A. R. P. acknowledges partial support by Collaborative Research Network grant 61 from the Inter-American Institute for Global Change Research. R. Matano's contribution was supported by the National Science Foundation grant OCE 0118363, NASA grant NAG5 12378, and JPL contract 1206714. This paper benefited substantially from comments and suggestions given by the anonymous reviewers. The authors would like to thank Andrés Rivas for kindly providing us the satellite data used in Figure 3.

References

Andersen, O. B., P. L. Woodworth, and R. A. Flather (1995), Intercomparison of recent ocean tide models, *J. Geophys. Res.*, *100*, 25,261–25,282.

Bakum, A., and R. H. Parrish (1991), Comparative studies of coastal pelagic fish reproductive habitats: The anchovy (Engraulis anchoita) of the southwestern Atlantic, *ICES J. Mar. Sci.*, *48*, 343–361.

Bisbal, G. A. (1995), The Southeast South American Shelf large marine ecosystem: Evolution and components, *Mar. Policy*, *19*(1), 21–38.

Blumberg, A. F., and G. L. Mellor (1987), A description of a three-dimensional coastal ocean circulation model, in *Three-Dimensional Coastal Ocean Models*, *Coastal Estuarine Sci. Ser.*, vol. 2, edited by N. Heaps, pp. 1–16, AGU, Washington D. C.

Boltovskoy, E. (1981), Masas de agua en el Atlántico Sudoccidental, in *Atlas del Zooplankton del Atl‡ntico Sudoccidental*, edited by D. Boltovskoy, pp. 227–237, Inst. Nac. Invest. Desarollo Pesquero, Mar del Plata, Argentina.

Carreto, J. I., V. A. Lutz, M. O. Carignan, A. D. Cucchi Colleoni, and S. G. De Marco (1995), Hydrography and clorophyll *a* in a transect from the coast to the shelf-break in the Argentinian Sea, *Cont. Shelf Res.*, *15*, 315–336.

Castro, B. M., and L. B. Miranda (1998), Physical oceanography of the western Atlantic continental shelf located between 4N and 34S, in *The Sea*, vol. 11, edited by A. R. Robinson and K. H. Brink, pp. 209–251, John Wiley, Hoboken, N. J.

Chelton, D. B., A. M. Mestas-Nuñez, and M. H. Freilich (1990), Global wind stress and Sverdrup circulation from the Seasat scatterometer, *J. Phys. Oceanogr.*, *20*, 1175–1205.

Davies, A. M., S. C. M. Kwong, and R. A. Flather (1997), A three-dimensional model of diurnal and semidiurnal tides on the European Shelf, *J. Geophys. Res.*, *102*, 8625–8656.

Egbert, G. D., and R. D. Ray (2001), Estimates of M2 tidal energy dissipation from TOPEX/Poseidon altimeter data, *J. Geophys. Res.*, *106*, 2475–2502.

Egbert, G. D., A. F. Bennet, and M. G. G. Foreman (1994), TOPEX/Poseidon tides estimated using a global inverse model, *J. Geophys. Res.*, *99*, 24,821–24,852.

Flather, R. A. (1976), A tidal model of the north-west European continental shelf, *Mem. Soc. R. Sci. Liege Ser. 6*, *10*, 141–164.

Flather, R. A. (1987), A tidal model of the northeast Pacific, *Atmos. Ocean*, *25*, 22–45.

Flather, R. A. (1988), A numerical model investigation of tides and diurnal period continental shelf waves along Vancouver Island, *J. Phys. Oceanogr.*, *18*, 115–139.

Forbes, M. C., and Z. D. Garraffo (1988), A note on the mean seasonal transport on the Argentinean shelf, *J. Geophys. Res.*, *93*, 2311–2319.

Genco, M. L., F. Lyard, and C. Le Provost (1994), The oceanic tides in the South Atlantic Ocean, *Ann. Geophys.*, *12*, 868–886.

Glorioso, P. D., and R. A. Flather (1995), A barotropic model of the currents off SE South America, *J. Geophys. Res.*, *100*, 13,427–13,440.

Glorioso, P. D., and R. A. Flather (1997), The Patagonian Shelf tides, *Prog. Oceanogr.*, *40*, 263–283.

Glorioso, P. D., and R. A. Simpson (1994), Numerical modelling of the M2 tide on the northern Patagonian Shelf, *Cont. Shelf Res.*, *14*, 267–278.

Guerrero, R. A., and A. R. Piola (1997), Masas de agua en la plataforma continental, in *El mar Agentino y sus recursos pesqueros*, vol. 1, edited by E. E. Boschi, pp. 107–118, Inst. Nac. Invest. Desarollo Pesquero, Mar del Plata, Argentina.

Han, G. (2000), Three-dimensional modeling of tidal currents and mixing quantities over Newfoundland Shelf, *J. Geophys. Res.*, *105*, 1407–1422.

Haney, R. L. (1991), On the pressure gradient force over steep topography in sigma coordinate ocean models, *J. Phys. Oceanogr.*, *21*, 610–619.

Hellerman, S., and M. Rosenstein (1983), Normal monthly wind stress over the World Ocean with error estimates, *J. Phys. Oceanogr.*, *13*, 1093–1104.

Höflich, O. (1984), Climate of the South Atlantic, in *Climates of the Oceans*, *World Surv. Climatol.*, vol. 15, edited by H. Van Loon, pp. 1–132, Elsevier Sci., New York.

Khanta, L. H. (1995), Barotropic tides in the global oceans from a nonlinear tidal model assimilating altimetric tides: 1. Model description and results, *J. Geophys. Res.*, *100*, 4653–4672.

Large, W. G., and H. van Loon (1989), Large scale, low frequency variability of the 1979 FGGE surface buoy drifts and winds over the Southern Hemisphere, *J. Phys. Oceanogr.*, *19*, 216–232.

Le Provost, C., M. L. Genco, F. Lyard, P. Vincent, and P. Canceil (1994), Spectroscopy of the world ocean tides from a finite element hydrodynamic model, *J. Geophys. Res.*, *99*, 24,777–24,797.

Lima, I. D., C. A. E. Garcia, and O. Moller (1996), Ocean surface processes on the southern Brazilian Shelf: Characterization and seasonal variability, *Cont. Shelf Res.*, *16*, 1307–1317.

Martos, P., and M. C. Piccolo (1988), Hydrography of the Argentine continental shelf between 38° and 42°S, *Cont. Shelf Res.*, *8*, 1043–1056.

O'Connor, W. P. (1991), A numerical model of tides and storm surges in the Rio de la Plata estuary, *Cont. Shelf Res.*, *11*, 1491–1508.

Orlanski, I. (1976), A simple boundary condition for unbounded hyperbolic flows, *J. Comput. Phys.*, *21*, 251–269.

Palma, E. D., and R. P. Matano (1998), On the implementation of passive open boundary conditions for a general circulation model: The barotropic mode, *J. Geophys. Res.*, *103*, 1319–1341.

Palma, E. D., and R. P. Matano (2000), On the implementation of open boundary conditions for a general circulation model: The three-dimensional case, *J. Geophys. Res.*, *105*, 8605–8627.

Panella, S., A. Michelato, R. Perdicaro, G. Magazzu, F. Decembrini, and P. Scarazzato (1991), A preliminary contribution to understanding the hydrological characteristics of the Strait of Magellan: Austral spring 1989, *Boll. Oceanol. Teor. Appl.*, *9*(2–3), 107–126.

Pereira, C. S. (1989), Seasonal variability in the coastal circulation on the Brazilian continental shelf (29°S–35°S), *Cont. Shelf Res.*, *9*, 285–299.

Piola, A. R., E. J. D. Campos, O. O. Moller, M. Charo, and C. Martinez (2000), Subtropical shelf front off eastern South America, *J. Geophys. Res.*, *105*, 6565–6578.

Rivas, A. L. (1997), Current meter observations in the Argentine continental shelf, *Cont. Shelf Res.*, *17*, 391–406.

Rivas, A. L., and A. Frank Langer (1996), Mass and heat transport in the Argentine continental shelf, *Cont. Shelf Res.*, *16*, 1283–1285.

Rodrigues, R. R., and J. A. Lorenzetti (2001), A numerical study of the effects of bottom topography and coastline geometry on the southeast Brazilian coastal upwelling, *Cont. Shelf Res.*, *21*, 371–393.

Sabatini, M., R. Reta, and R. Matano (2004), Circulation and zooplankton biomass distribution over the southern Patagonian Shelf during late summer, *Cont. Shelf Res.*, *24*, 1359–1373.

Schwiderski, E. W. (1980), Ocean tides, 2, A hydrodynamical interpolation model, *Mar. Geod.*, *3*, 218–257.

Sharples, J., and J. H. Simpson (1996), The influence of the spring-neaps cycle on the position of shelf sea fronts, in *Buoyancy Effects on Coastal and Estuarine Dynamics*, *Coastal Estuarine Stud.*, vol. 53, edited by D. G. Aubrey and C. T. Friedrichs, pp. 71–82, AGU, Washington, D. C.

Smith, R. D., and D. T. Sandwell (1997), Global sea floor topography from satellite altimetry and ship depth soundings, *Science*, *277*, 1956–1962.

Trenberth, K. E., W. G. Large, and J. G. Olson (1990), The mean annual cycle in global wind stress, *J. Phys. Oceanogr.*, *20*, 1742–1760.

Zavialov, P., O. Moller, and E. Campos (2002), First direct measurements of currents on the continental shelf of southern Brazil, *Cont. Shelf Res.*, *22*, 1975–1986.

R. P. Matano, College of Oceanic and Atmospheric Sciences, Oregon State University, Corvallis, OR 97331-5503, USA. (rmatano@oce.orst.edu)

E. D. Palma, Departamento de Física, Universidad Nacional del Sur, Avda. Alem 1253, 8000 Bahía Blanca, Argentina. (uspalma@criba.edu.ar)

A. R. Piola, Departamento de Oceanografía, Servicio de Hidrografía Naval, 1271 Buenos Aires, Argentina. (apiola@hidro.gov.ar)